# SUPPORTING INFORMATION

# Electronic Transport in CdSe Nanoplatelet Based Polymer Fibres

*Jan F. Miethe‡, Anja Schlosser‡, J. Gerrit Eckert, Franziska Lübkemann, Nadja C. Bigall\**

Institute of Physical Chemistry and Electrochemistry, Leibniz Universität Hannover,

Callinstr. 3a, D-30167 Hannover, Germany

## 1. Platelet characterisation
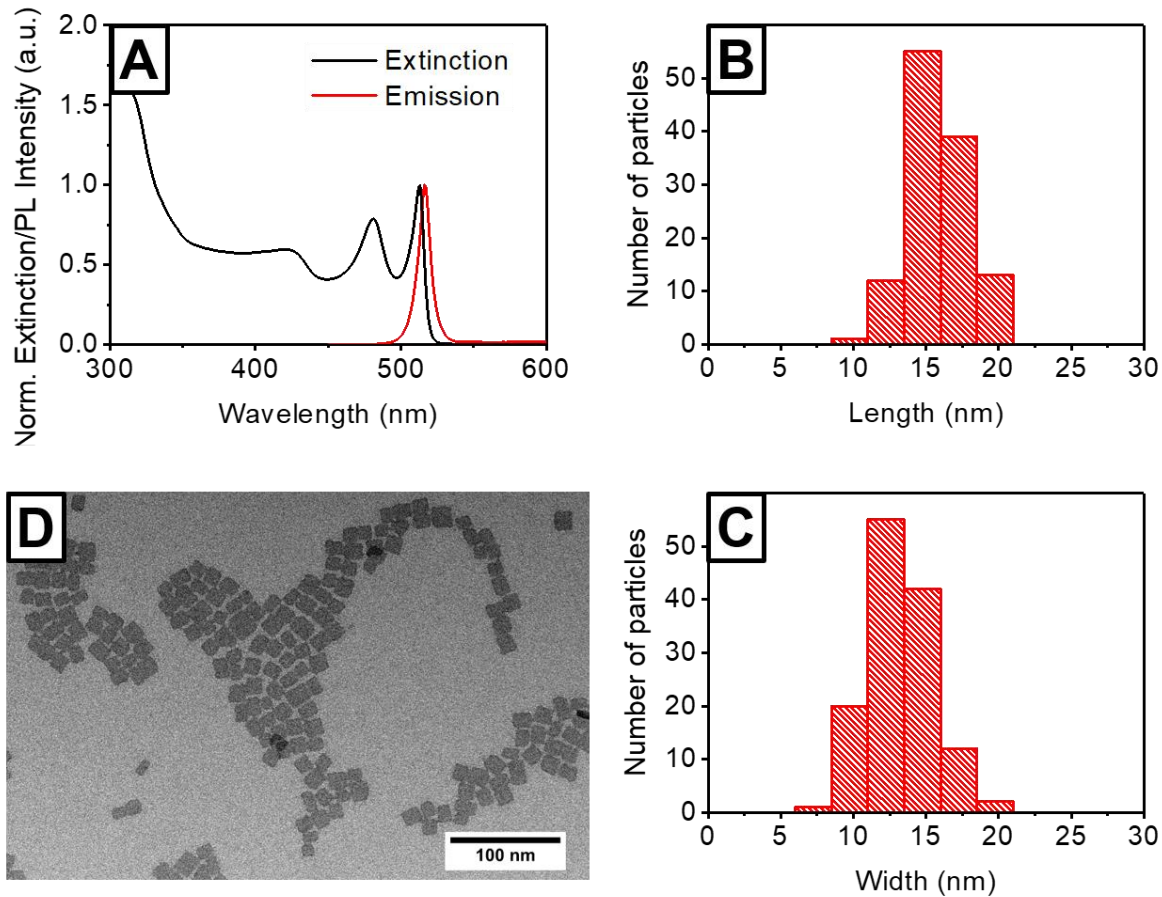


**Figure S1.** (A) Optical spectra of 4 ML CdSe NPLs: extinction (black) and PL emission (red). (B) and (C) Distribution of platelet length (longer edge) and platelet width (shorter edge) derived from TEM images. (D) TEM micrograph of 4 ML CdSe NPLs.

Quasi-quadratic CdSe NPLs with a thickness of 4 MLs have been synthesised according to a previously published protocol[1]. The thickness of CdSe NPLs can be derived from their optical spectra.[2,3] In the UV/Vis extinction spectrum, two well-pronounced maxima at 481 nm and 513 nm, corresponding to the light hole-electron and the heavy hole-electron transition of 4 ML thick platelets,[3] are visible. The PL emission spectrum shows one peak at 516 nm with a full width at half maximum (FWHM) of 10 nm, confirming the NPL thickness to be 4 MLs[3]. From the TEM micrographs, an approximate thickness of 2.0 nm $\pm$ 0.2 nm was determined, what is much higher than reported in the literature (1.22 nm).[3] This observation might have been caused by the fact that the NPLs did not stand ideally perpendicular to the TEM grid. However, the TEM micrographs showed that quasi-quadratic NPLs with average dimensions of 16.6 nm $\pm$ 2.3 nm x 13.2 nm $\pm$ 1.7 nm were obtained. No impurities were observed.

## 2. Preparation and optical characterization of hybrid structures

The CdSe NPL-polymer hybrid structures were synthesised according to a procedure previously developed for quasi-spherical magnetic nanoparticles[4] with some modifications. In the hybrid structures, the platelets are highly ordered in stacks, which are often parallel to each other. Some of the stacks are not perfectly perpendicular to the TEM grid and appear more diffuse than others. Due to the TEM sample preparation method, network-like structures are formed out of the single fibres (probably drying effects). The distances between the platelets can be derived from the high resolution (HR)-TEM images shown in Figure 2 D+E. Centre-to-centre distances of 3.94 nm ± 0.23 nm were measured. Compared to the distances between stacked, oleic acid coated platelets reported so far (Table S1), the values observed in our experiments are distinctly lower. To date, stacked superstructures were either synthesised by antisolvent addition[1,5,6] or by drying of a hexane NPL solution and subsequent

**Table S1.** Results of different studies on stacking of CdSe NPLs. The applied surface ligands/polymers are abbreviated as follows: OA = oleic acid, HA = heptanoic acid, OC = octanoic acid, SBS = styrene-butadiene-styrene block copolymer.

| NPL type-surface ligand formation conditions | Platelet distance / nm | | Measurement technique | Reference |
| --- | --- | --- | --- | --- |
| | centre-to-centre | surface-to-surface | | |
| CdSe 4 ML quasi-quadratic-OA antisolvent addition (hexane/EtOH) | 5.1 | 3.9 | SAXS | 1 |
| CdSe 4 ML quasi-quadratic-OA antisolvent addition (hexane/EtOH) | 4.29 ± 0.36 | 3.09 | HR-TEM | 5 |
| CdSe 4 ML quasi quadratic-OA drying from hexane solution | 5.27 | 4.07 | SAXS | 7 |
| CdSe 4 ML quasi quadratic-HA drying from hexane solution | 3.3 | 2.1 | SAXS | 7 |
| CdSe 5 ML quasi rectangular-OA drying from hexane solution | 5.84 | 4.34 | SAXS | 8 |
| CdSe 5 ML quasi rectangular-OA antisolvent addition (hexane/EtOH) | 5.1 | 3.6 | SAXS | 6 |
| CdSe 5 ML quasi rectangular-OC antisolvent addition (hexane/EtOH) | 3.8 | 2.3 | SAXS | 6 |
| CdSe 4 ML quasi quadratic-OA solvent-casting of NPL/SBS film | 5.7 | 4.5 | SAXS | 9 |

| NPL type-surface ligand formation conditions | Platelet distance / nm | | Measurement technique | Reference |
|---|---|---|---|---|
| | centre-to-centre | surface-to-surface | | |
| CdSe 4 ML quasi-quadratic-OA antisolvent (THF/ACN) and polymer addition (PMAO) | $3.94 \pm 0.23$ | 2.74 | HR-TEM | this work |

redispersion of the superstructures[7,8]. In one case, stacked CdSe NPLs were embedded into a polymer matrix.[9] The surface-to-surface distances between the stacked NPLs range from 2.1 nm to 4.5 nm. The chain length of the NPL surface ligands was identified to be the main influencing factor of the NPL-NPL distance.[6,7] For oleic acid coated NPLs, a maximum surface-to-surface distance of 4.5 nm was observed, which is still less than the length of two fully stretched oleic acid molecules.[1] In our case, surface-to-surface distances of slightly more than the length of one oleic acid molecule were measured, indicating that there are strong attractive forces between neighbouring NPLs. We suppose that the NPLs are pushed closer together due to depletion attraction, induced by the addition of polymer. Low distances of the NPLs inside the stacks are beneficial for the charge carrier transport between the NPLs,[5] and should therefore also enhance the electrochemical performance of the fibres.

To learn more about the hybrid structure formation mechanism, several synthesis parameters were varied. At first, the amount of polymer added during the experiment was varied. TEM micrographs of the synthesised fibres are shown in Figure 3.

Moreover, the amount of ACN in the synthesis was varied. If no ACN at all is added, NPL stacks surrounded by a polymer shell are still formed, however, they are strongly aggregated (Figure S2). It is moreover noticeable, that the NPL-NPL distance increased slightly (4.07 nm $\pm$ 0.21 nm) compared to the original procedure (for details, see Experimental Section). This observation supports our theory, that the polymer encapsulated stacks are formed through the contribution of two different forces, which are destabilisation due to an increase in the polarity of the solution, and depletion attraction.
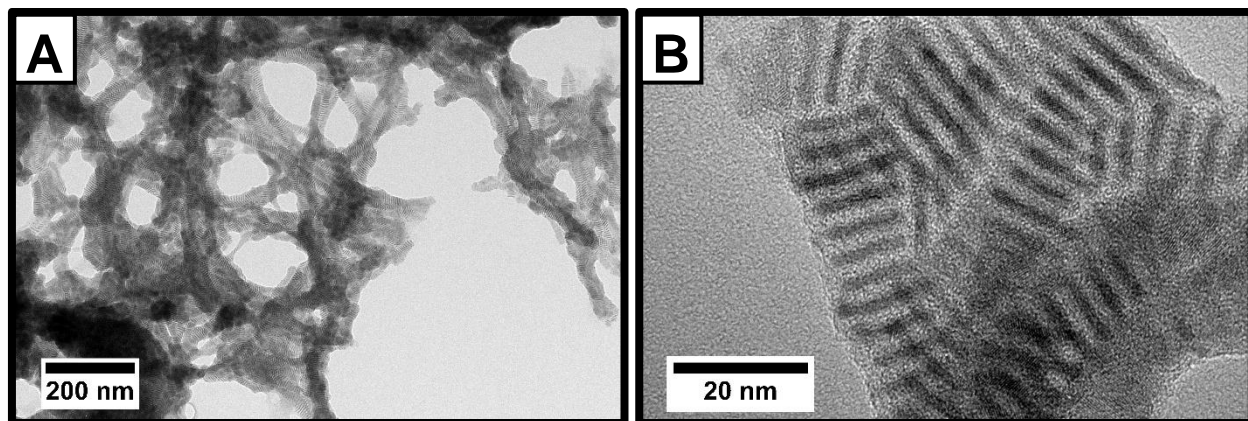
**Figure S2.** TEM micrographs of NPL/polymer hybrid structures synthesised without additional ACN in lower (A) and higher magnification (B).

Additionally, the influence of the polymer purity, especially of its water content, was studied. Therefore, two different batches of PMAO were applied in the synthesis of the fibres. One batch was opened and stored in a glove box under an inert atmosphere (PMAO-i), whereas the other batch was stored under ambient conditions for more than four years (PMAO-a). As can be seen from the TEM images (Figure S3 A+B) of PMAO-a coated NPL stacks, much longer fibres were obtained if PMAO-a is applied in the synthesis. The fibre as well as the polymer thickness, however, were nearly similar to PMAO-i coated fibres (Figure 2 B-E). Both polymers mainly differed in their water content, which was proven by thermogravimetric analysis (TGA) and nuclear magnetic resonance (NMR). Applying TGA, water contents of 0.2 % and 1.5 % were determined for PMAO-i and PMAO-a, respectively. In the NMR spectra, no structural changes of the polymer were observed. These results imply that even very small differences in the water amount during the hybrid structure synthesis strongly influence the appearance of the product.
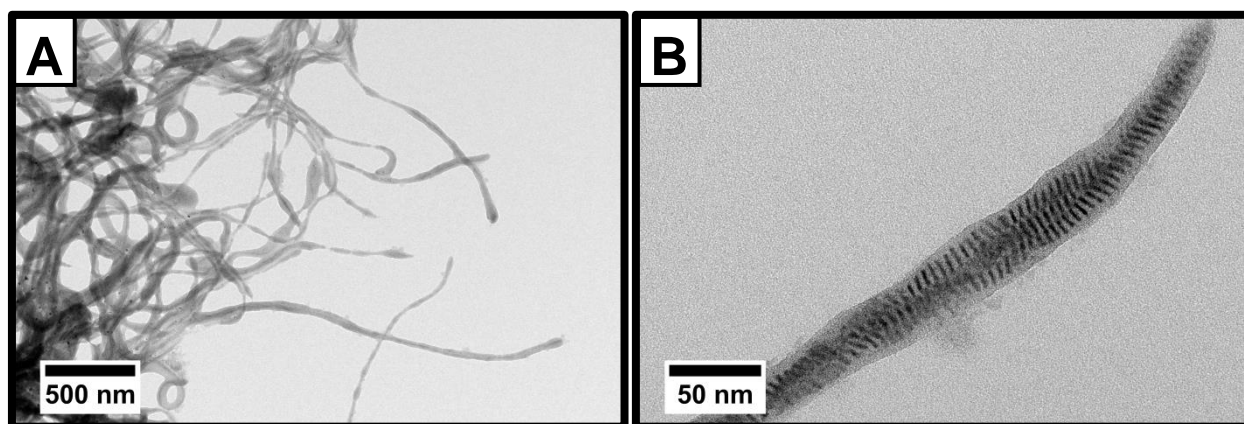


**Figure S3.** TEM micrographs of NPL/polymer hybrid structures synthesised with PMAO-a in lower (A) and higher magnification (B).

Finally, the NPL thickness and shape was varied in order to demonstrate the universality of the developed polymer coating procedure. For this purpose, quasi-rectangular NPLs with two different thicknesses (4 and 5 ML) were chosen. The platelets were synthesised according to literature methods[10,11] and characterised by fluorescence emission spectroscopy (Figure S4 D) and TEM (Figure S4 B+C right). Afterwards, they were employed in the fibre synthesis as described in the Experimental Section without any modifications. In both cases, the formation of anisotropic fibres comparable to those obtained with quasi-quadratic 4 ML NPLs was observed, as can be derived from the TEM images (Figure S4 B+C middle/left). Moreover, it is noticeable that fibres made out of NPLs with distinctly higher aspect ratios (ARs) than one are often twisted and form less ordered structures. The latter observation might be explained with the fact that the synthesis procedure and especially the concentrations of the different reagents were not modified although NPLs with other dimensions were used.
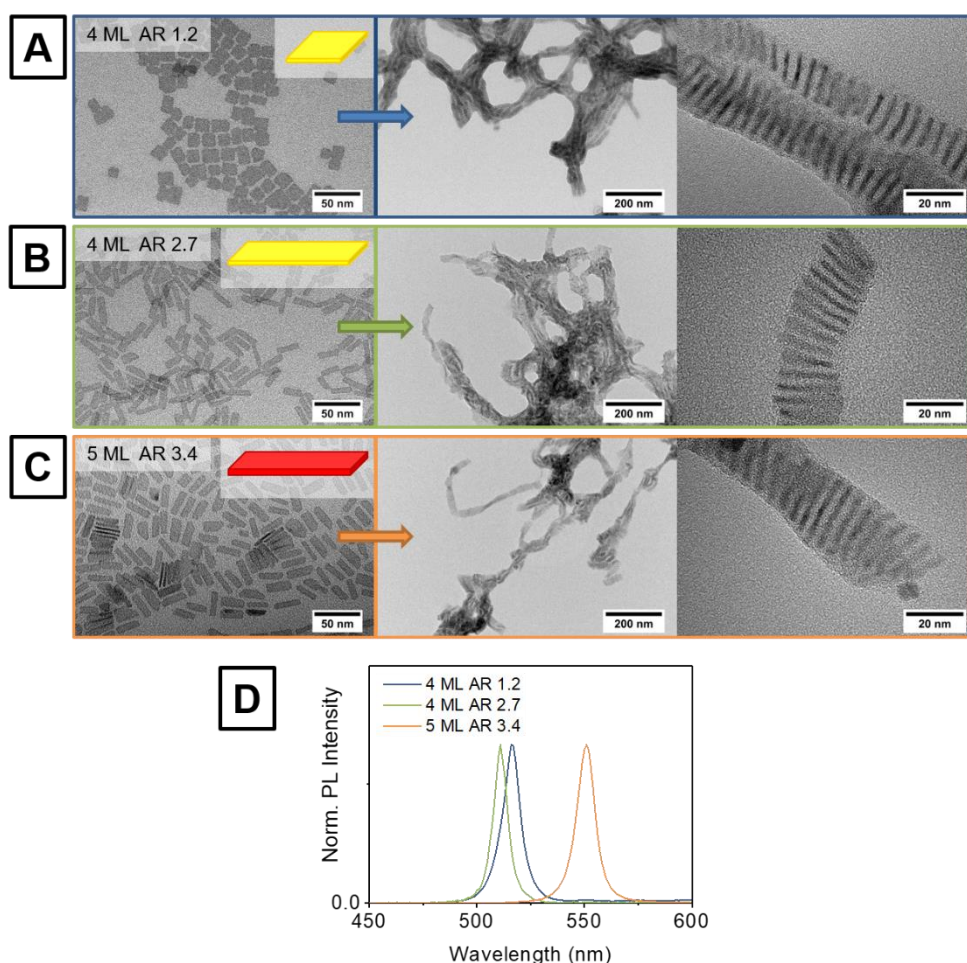


**Figure S4.** TEM micrographs of fibres based on 4 ML quasi-quadratic NPLs with an aspect ratio (AR) of nearly one (A), 4 ML quasi-rectangular NPLs with an aspect ratio of 2.7 (B), and 5 ML quasi-rectangular NPLs with an aspect ratio of 3.4 (C). (D) PL emission spectra of the hexane based NPL solutions before fibre synthesis.

The hybrid structures were moreover characterised by UV/Vis extinction (Figure S5) and UV/Vis absorption spectroscopy (Figure S6). In both spectra of the hybrid structures, the characteristic peaks of CdSe NPLs are visible. The maximum corresponding to the light hole-electron transition is slightly shifted to longer wavelengths by 1 nm compared to the pristine NPLs. Moreover, a broadening of both maxima is visible. Due to the size of the hybrid structures being in the range of micrometres, a strong background absorption originating from light scattering is present in the extinction spectrum.
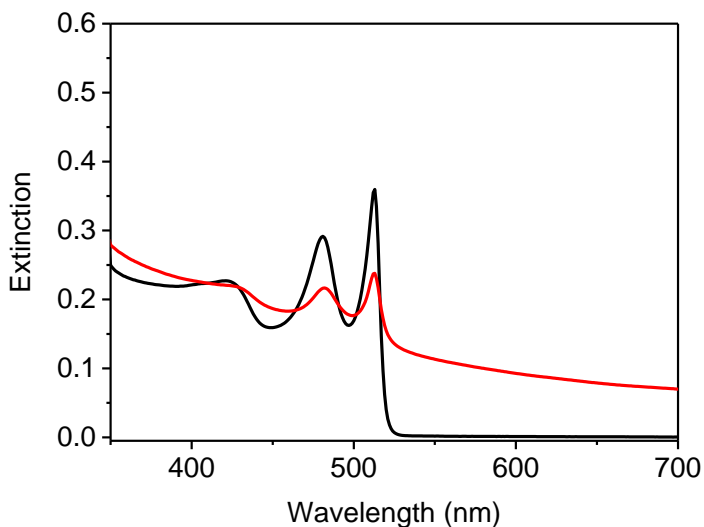


**Figure S5.** UV/Vis extinction spectra of pristine CdSe NPLs (black line) and NPL/polymer hybrid structures (red line). The spectra were measured in hexane and aqueous KOH, respectively.
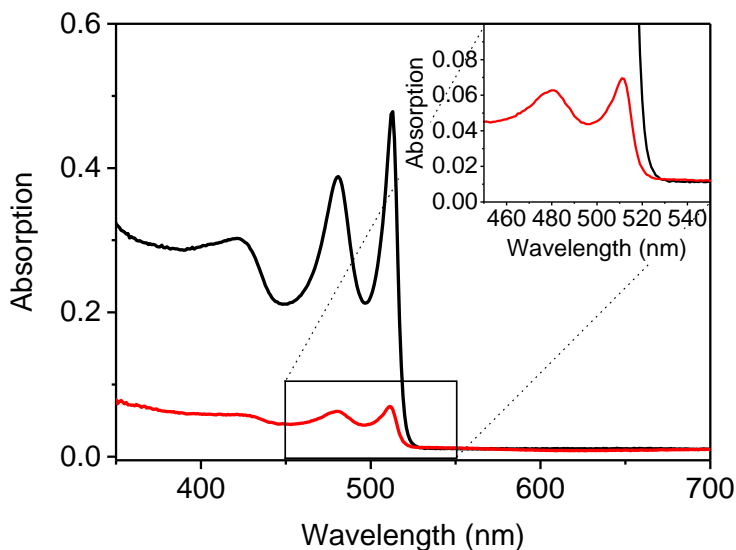


**Figure S6.** UV/Vis absorption spectra of pristine CdSe NPLs (black line) and NPL/polymer hybrid structures (red line). The spectra were measured in an integrating sphere.

Finally, X-ray diffraction patterns of the pristine NPLs, the NPL/polymer fibres, and the polymer were recorded (Figure S7).
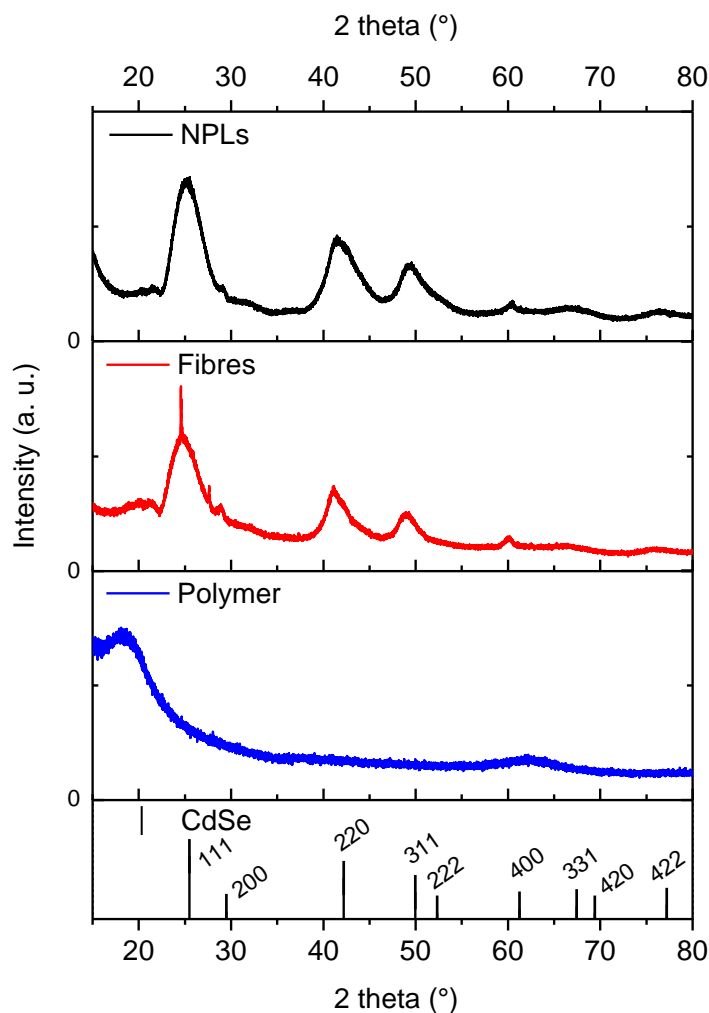


**Figure S7.** X-ray diffraction patterns of pristine 4 ML CdSe NPLs (top), NPL/polymer fibres (second from top), and PMAO (second from bottom). On the bottom, the reflection intensities and positions of bulk CdSe with zinc blende structure are shown (JCPDS Powder Diffraction File # 03-065-2891).

The XRD pattern of the CdSe NPLs (Figure S7 top) confirms that CdSe NPLs with cubic zinc blende structure have been obtained. Due to the small particle size, all reflections are strongly broadened, but the positions and intensities of the reflections approximately match the literature pattern. The XRD pattern of the fibres differs only slightly from the pattern of the pristine NPLs. At 2 theta values of 24.6 ° and 27.6 ° two sharp reflections are observed, which are probably caused by an impurity. These reflections were observed in the XRD patterns of all investigated fibre samples, but their percentage differed. It is therefore likely that these reflections correspond to a substance formed during the fibre synthesis or purification process, *e. g.* a potassium salt.

## 3. Characterisation of photoelectrodes
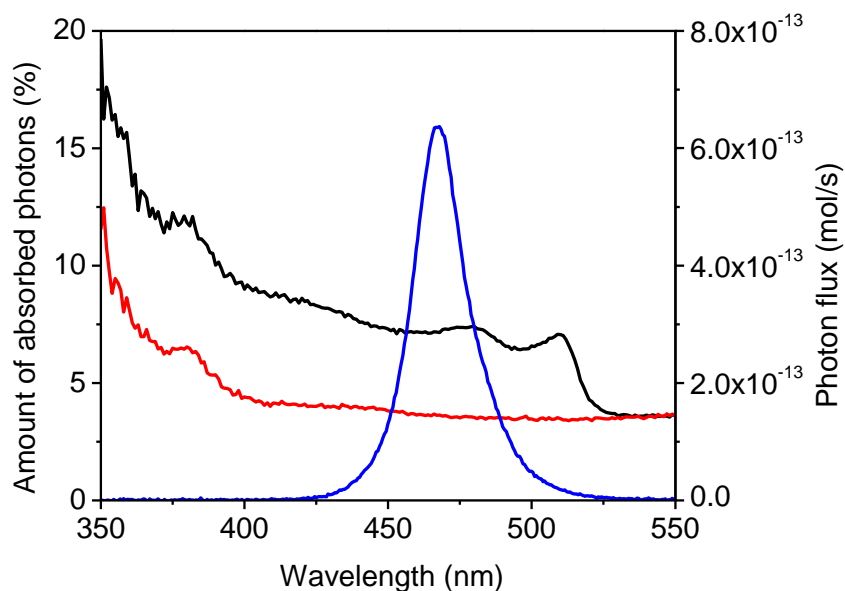


**Figure S8.** UV/Vis absorption spectra of NPL/polymer hybrid structures (black line) on an ITO electrode and a blank ITO electrode (red line). The mismatch between both spectra is caused by NPL/polymer hybrid structures. The photon flux of the LED applied for kinetic measurements (blue line) overlaps with the absorption of the hybrid structure coated electrodes.
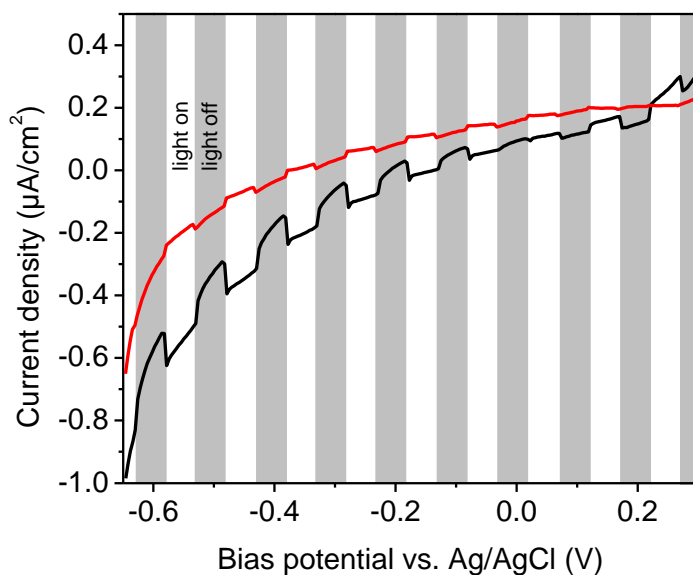


**Figure S9.** Linear sweep voltammograms of pristine NPLs (black line) and NPL/polymer hybrid structures (red line) adsorbed on ITO glass slides. During the measurement, the samples were periodically illuminated by a blue LED ($T = 25$ s). The grey regions correspond to the periods, in which the LED was switched off, the white regions correspond to the on-periods.
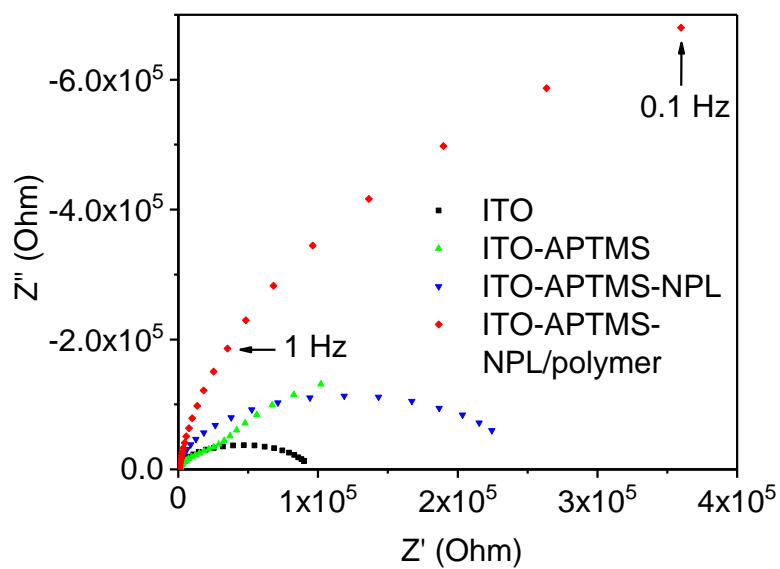
**Figure S10.** Impedance spectra of pure ITO slides (black), APTMS functionalised ITO slides (green), APTMS functionalised slides with adsorbed NPLs (blue), and APTMS functionalised slides with adsorbed NPL/polymer hybrid structures (red). The measurements were carried out at a bias potential of 300 mV with a modulation of 20 mV in the frequency range between 10 kHz to 0.1 Hz.

## 4. Details on photoelectrochemical setup
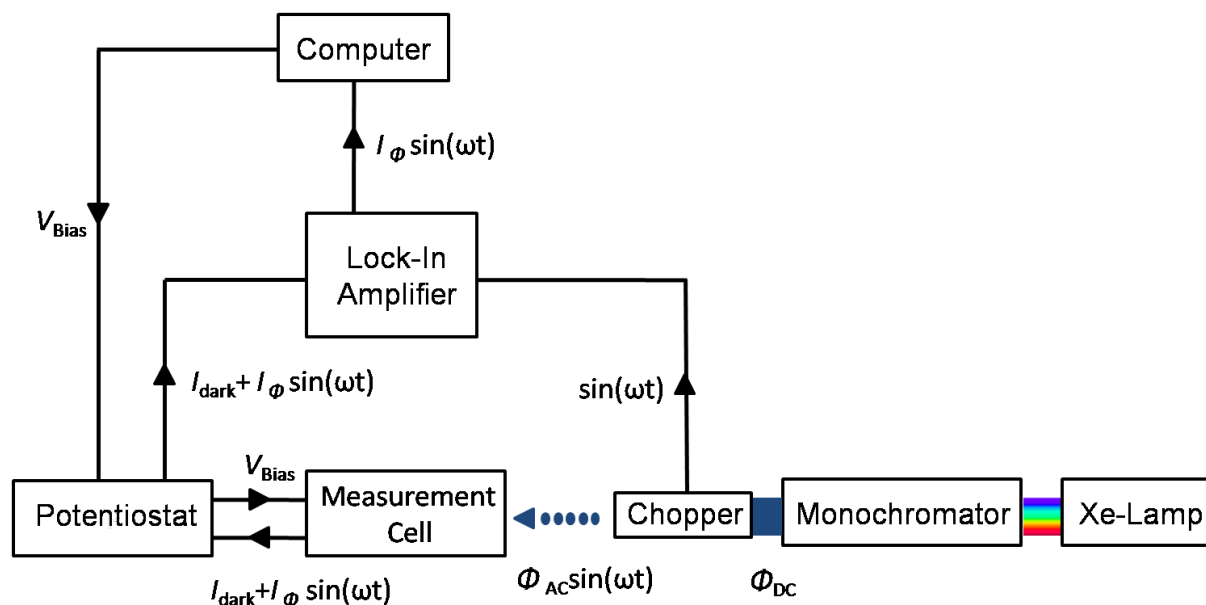


**Figure S11.** Scheme of the measurement setup for determination of wavelength specific photocurrents. The applied monochromator was adjusted to a slit width of 5 nm.
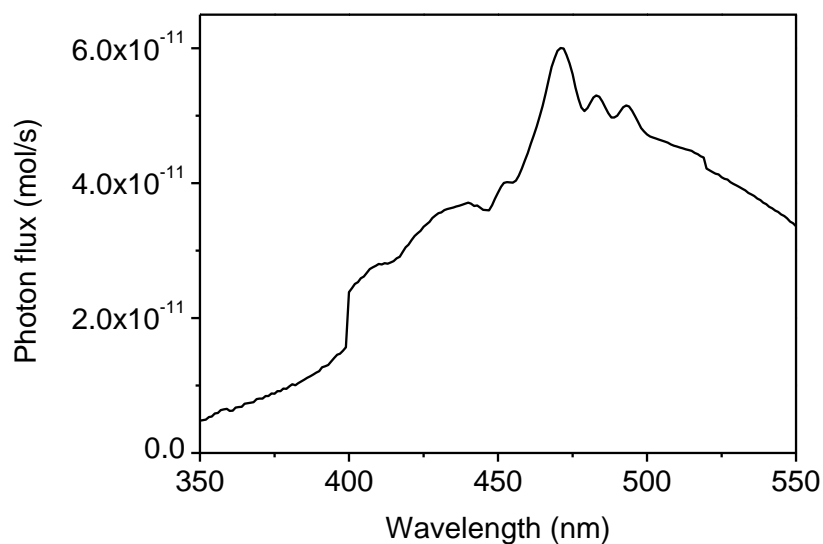


**Figure S12.** Photon emission of the applied Xe-lamp-monochromator setup, which was used to record external photocurrent quantum efficiency spectra. The spectrum was measured with a FDS-100-Si-PD Si-photodiode from THORLabs. It shows the characteristic peaks of a Xe-lamp light source and a step caused by the monochromator grating change at 400 nm.
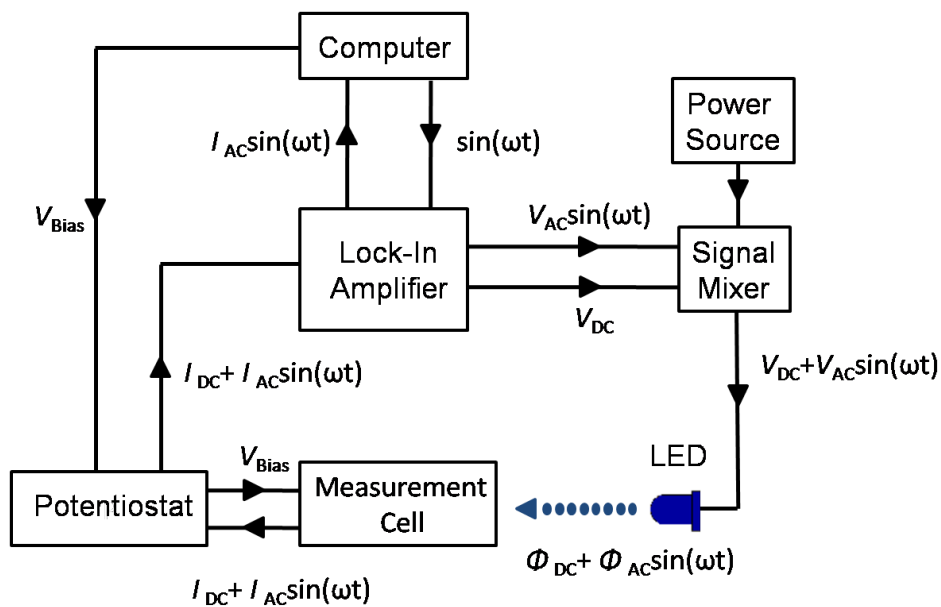
**Figure S13.** Scheme of the measurement setup for determination of intensity modulated photocurrent spectra.
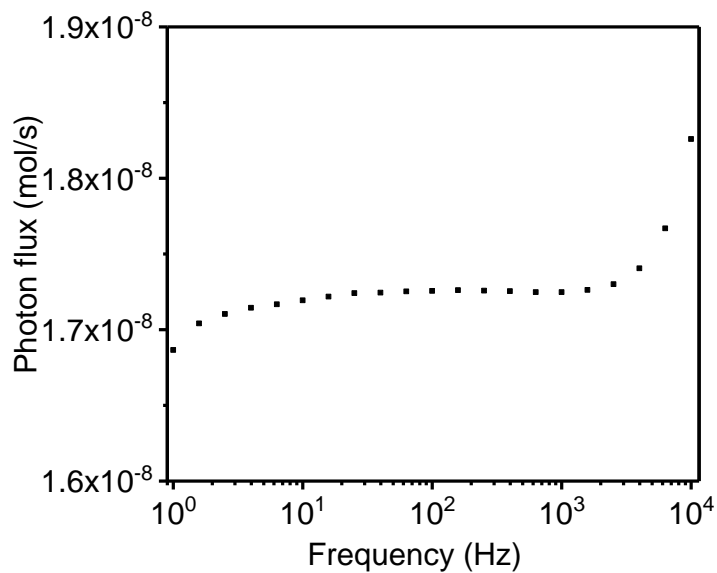


**Figure S14.** Photon flux of the LED ($\lambda = 468$ nm) applied in the IMPS experiments in relation to the applied frequency.

**Table 2.** Exemplary calculation of the energy output of the applied Xe-lamp-monochromator setup determined by a Si-photodiode.

| Wavelength (nm) | Energy of a photon (J) | Photocurrent (A) | Sensitivity of photodiode (A/W) | Energy output of setup (W) |
|---|---|---|---|---|
| 475 | $4.2 \times 10^{-19}$ | $3.3 \times 10^{-9}$ | 0.144 | $2.29 \times 10^{-8}$ |

**Table 3.** Exemplary calculation of the photon flux of the applied Xe-lamp-monochromator setup at a specific wavelength.

| Number of photons before correction | Number of photons before correction (mol) | Correction factor of OD filters | Number of photons (mol) |
|---|---|---|---|
| $5.4 \times 10^{10}$ | $9.06 \times 10^{-14}$ | $1.624 \times 10^{-3}$ | $5.58 \times 10^{-11}$ |

References:

(1)     Abécassis, B.; Tessier, M. D.; Davidson, P.; Dubertret, B. *Nano Lett.* **2014**, *14* (2), 710–715.

(2)     Ithurria, S.; Dubertret, B. *J. Am. Chem. Soc.* **2008**, *130* (49), 16504–16505.

(3)     Ithurria, S.; Tessier, M. D.; Mahler, B.; Lobo, R. P. S. M.; Dubertret, B.; Efros, A. L. *Nat. Mater.* **2011**, *10* (12), 936–941.

(4)     Bigall, N. C.; Wilhelm, C.; Beoutis, M.-L.; García-Hernandez, M.; Khan, A. A.; Giannini, C.; Sánchez-Ferrer, A.; Mezzenga, R.; Materia, M. E.; Garcia, M. A.; Gazeau, F.; Bittner, A. M.; Manna, L.; Pellegrino, T. *Chem. Mater.* **2013**, *25* (7), 1055–1062.

(5)     Guzelturk, B.; Erdem, O.; Olutas, M.; Kelestemur, Y.; Demir, H. V. *ACS Nano* **2014**, *8* (12), 12524–12533.

(6)     Tessier, M. D.; Biadala, L.; Bouet, C.; Ithurria, S.; Abecassis, B.; Dubertret, B. *ACS Nano* **2013**, *7* (4), 3332–3340.

(7)     Jana, S.; Phan, T. N. T.; Bouet, C.; Tessier, M. D.; Davidson, P.; Dubertret, B.; Abécassis, B. *Langmuir* **2015**, *31* (38), 10532–10539.

(8)     Jana, S.; de Frutos, M.; Davidson, P.; Abécassis, B. *Sci. Adv.* **2017**, *3* (9), e1701483.

(9)     Beaudoin, E.; Abecassis, B.; Constantin, D.; Degrouard, J.; Davidson, P. *Chem. Commun.* **2015**, *51* (19), 4051–4054.

(10)    Naskar, S.; Schlosser, A.; Miethe, J. F.; Steinbach, F.; Feldhoff, A.; Bigall, N. C. *Chem. Mater.* **2015**, *27* (8), 3159–3166.

(11)    Pedetti, S.; Ithurria, S.; Heuclin, H.; Patriarche, G.; Dubertret, B. *J. Am. Chem. Soc.* **2014**, *136* (46), 16430–16438.